LANCZOS-BASED EXPONENTIAL FILTERING FOR DISCRETE ILL-POSED PROBLEMS

D. CALVETTI * AND L. REICHEL †

In memory of Rüdiger Weiss.

Abstract. We describe regularizing iterative methods for the solution of large ill-conditioned linear systems of equations that arise from the discretization of linear ill-posed problems. The regularization is specified by a filter function of Gaussian type. A parameter μ determines the amount of regularization applied. The iterative methods are based on a truncated Lanczos decomposition and the filter function is approximated by a linear combination of Lanczos polynomials. A suitable value of the regularization parameter is determined by an L-curve criterion. Computed examples that illustrate the performance of the methods are presented.

Key words. iterative method, regularization, exponential filter function

AMS subject classifications. 65F22, 65F10, 65D15

1. Introduction. This paper is concerned with the computation of an approximate solution of linear systems of equations

$$Ax = \tilde{g}, \qquad A \in \mathbb{R}^{n\times n}, \qquad \tilde{g} \in \mathbb{R}^n, \tag{1}$$

where A is a large symmetric matrix with many eigenvalues of different orders of magnitude close to the origin; some of the eigenvalues may vanish. The available right-hand side vector $\tilde{g}$ is assumed to be an approximation of an unknown vector g' in the range of A. The difference

$$e := \tilde{g} - g' \tag{2}$$

may stem from measurement or discretization errors and will be referred to as noise. The vector $\tilde{g}$ is not required to be in the range of A.

Linear systems of equations with these properties arise when discretizing linear ill-posed problems, such as Fredholm integral equations of the first kind with a smooth symmetric kernel. Following Hansen [14], we refer to such linear systems of equations as linear discrete ill-posed problems.

This paper presents new iterative methods for the solution of large linear discrete ill-posed problems with a symmetric matrix, which may be definite, indefinite or singular.

Consider the consistent linear system of equations with the noise-free right-hand side g',

$$Ax = g', \tag{3}$$

associated with (1). We would like to determine the solution of minimal Euclidean norm, denoted by x', of this system. However, the right-hand side g' in (3) is not available. Therefore, we seek to determine an approximation of x' by computing an

*Department of Mathematics, Case Western Reserve University, Cleveland, OH 44106. E-mail dxc57@po.cwru.edu. This work was in part supported by NSF grant DMS-9806702.

†Department of Mathematics and Computer Science, Kent State University, Kent, OH 44242. E-mail reichel@mcs.kent.edu. This work was in part supported by NSF grant DMS-9806413.

approximate solution of the linear system of equations (1) with known right-hand side $\tilde{g}$.

Due to the noise e in $\tilde{g}$ and the severe ill-conditioning of the matrix A, straightforward solution of (1) typically does not yield a meaningful approximation of x'. In order to facilitate the computation of a meaningful approximation of x', one generally replaces the discrete ill-posed problem (1) by a related problem that is less sensitive to the noise e in $\tilde{g}$, and then solves the problem obtained for an approximation of x'. This replacement is referred to as regularization. We propose to replace the discrete ill-posed problem (1) by the least-squares problem

$$\min_{x\in\mathbb{R}^n} \|Ax - \varphi_\mu(A)\tilde{g}\|, \tag{4}$$

where $\|\cdot\|$ denotes the Euclidean vector norm and $\varphi_\mu(t)$ is a filter function of Gaussian type,

$$\varphi_\mu(t) := 1 - \exp(-\mu t^2). \tag{5}$$

It is the purpose of this function to "filter out" the contributions of the noise e in $\tilde{g}$ to the computed solution. The nonnegative regularization parameter μ determines how much noise is filtered out. Regularization by filtering out noise in the given data $\tilde{g}$ is sometimes referred to as prewhitening; see Louis [16] for a recent discussion of prewhitening and its relation to other regularization methods.

Let $A^\dagger$ denote the Moore-Penrose pseudo-inverse of the matrix A. The least-squares solution of minimal Euclidean norm of (4) is given by

$$x_\mu = \varphi_\mu(A)A^\dagger\tilde{g}. \tag{6}$$

Note that $x_\infty = A^\dagger\tilde{g}$, i.e., when $\mu = \infty$ the minimal-norm solution of (4) agrees with the minimal-norm least-squares solution of (1). This solution generally is a poor approximation of x', because the noise e in the right-hand side $\tilde{g}$ is not filtered out. On the other hand, the choice $\mu = 0$ filters out too much; both e and $\tilde{g}$ are filtered out and we obtain $x_0 = 0$, which in general is a poor approximation of x'. The determination of a suitable value of the regularization parameter is an important problem. Hansen [12] proposed that an L-curve be used for this purpose. Section 4 describes how the L-curve criterion conveniently can be used for the iterative methods of the present paper.

The influence of the filter function on the solution x_μ for $0 < \mu < \infty$ can easily be seen by substituting the spectral factorization

$$A = U_n\Lambda_n U_n^*, \qquad U_n^*U_n = I_n, \qquad \Lambda_n = \mathrm{diag}[\lambda_1, \lambda_2, \ldots, \lambda_n], \tag{7}$$

into (6). Here I_n is the $n \times n$ identity matrix and the superscript $*$ denotes transposition. For future reference, we introduce the index sets

$$\mathcal{J}_0(A) := \{j : \lambda_j = 0\}, \qquad \mathcal{J}_1(A) := \{j : \lambda_j \neq 0\}. \tag{8}$$

Let U_n have columns u_j and define

$$\delta_j := u_j^*\tilde{g}, \qquad 1 \leq j \leq n.$$

Then equation (6) can be expressed as

$$x_\mu = \sum_{j\in\mathcal{J}_1(A)} \varphi_\mu(\lambda_j)\frac{\delta_j}{\lambda_j}u_j. \tag{9}$$

This representation of x_μ shows that for $0 < \mu < \infty$, eigenvector components of x_μ associated with eigenvalues of small magnitude are damped, while eigenvector components associated with eigenvalues of large magnitude are not damped significantly. The smaller the value of μ, the more damping.

Application of the filter function (5) to the solution of ill-posed problems was proposed in [3]. Other choices of filter functions have been described in the literature. For instance, the simplest form of Tikhonov regularization applied to (1) yields the linear system of equations

$$(A^2 + \frac{1}{\mu} I_n)x = A\tilde{g}$$

with solution

$$x_\mu^T = \varphi_\mu^T(A)A^\dagger \tilde{g},$$

where the Tikhonov filter function is given by

$$\varphi_\mu^T(t) := 1 - \frac{1}{1 + \mu t^2} \tag{10}$$

and $\mu > 0$ is the regularization parameter. Note that when μt^2 is sufficiently small, the exponential filter function $\varphi_\mu(t)$ is an accurate approximation of the Tikhonov filter function (10). On the other hand, for μ fixed, the Tikhonov filter function has singularities at the points $t := \pm i/\sqrt{\mu}$ in the complex plane, where $i := \sqrt{-1}$, while the exponential filter function (5) is analytic in the finite complex plane. We refer to [5] for further discussions on the filter function (10). Numerical examples that compare the filtering properties of the exponential and Tikhonov filter functions, as well as of the filter function defined by truncated singular value decomposition, are presented in [1].

The present paper develops an iterative method for computing an approximation of x_μ by determining polynomial approximants of the function $t^{-1}\varphi_\mu(t)$. The approximants are expressed as a linear combination of orthogonal polynomials that are determined by the Lanczos process when applied to the matrix A with initial vector $\tilde{g}$. The rapid convergence of the polynomial approximant follows from the fact that the function $t^{-1}\varphi_\mu(t)$ is analytic in the whole complex plane.

We remark that if a bounded interval $[a, b]$ that contains the spectrum of the matrix A is known, then it is possible to determine polynomial approximants of $t^{-1}\varphi_\mu(t)$ on $[a, b]$ by expanding this function in terms of Chebyshev polynomials for this interval. An iterative method based on this approach is presented in [4].

This paper is organized as follows. Section 2 describes a new iterative method for approximating the vector x_μ defined by (6) for a fixed value of the regularization parameter $\mu > 0$. A modification of this method that secures that the computed approximate solutions of (4) are orthogonal to the null space of A is presented in Section 3. The choice of a suitable value of the regularization parameter μ is discussed in Section 4, and a few computed examples are presented in Section 5. Finally, Section 6 contains concluding remarks.

2. An exponentially filtering iterative method. We derive an iterative method based on the Lanczos process for computing approximations of the vector x_μ defined by (6). The method determines a polynomial approximant of the analytic

function

$$\psi_\mu(t) := \begin{cases} t^{-1}(1-\exp(-\mu t^2)), & t \neq 0, \\ 0, & t = 0. \end{cases} \tag{11}$$

Note that the solution (6) of the least-squares problem (4) can be expressed as

$$x_\mu = \psi_\mu(A)\tilde{g}. \tag{12}$$

Application of m steps of the Lanczos process to the matrix A with initial vector $\tilde{g}$ yields the decomposition

$$AQ_m = Q_m T_m + q'_m e_m^*, \tag{13}$$

where the matrix $Q_m = [q_0, q_1, \ldots, q_{m-1}] \in \mathbb{R}^{n\times m}$ satisfies $Q_m^* Q_m = I_m$ and $Q_m e_1 = \tilde{g}/\|\tilde{g}\|$, the matrix $T_m \in \mathbb{R}^{m\times m}$ is symmetric and tridiagonal with nonvanishing subdiagonal elements, the vector $q'_m \in \mathbb{R}^n$ is orthogonal to the columns of Q_m, and e_j denotes the jth axis vector. Throughout this paper, we assume that the Lanczos process does not break down during the first m steps. In the rare event of a breakdown, the formulas derived can be simplified in an obvious manner.

It follows from (13) that the columns q_j of the matrix Q_m span the Krylov subspace

$$\mathcal{K}_m(A, \tilde{g}) := \text{span}\{\tilde{g}, A\tilde{g}, A^2\tilde{g}, \ldots, A^{m-1}\tilde{g}\} \tag{14}$$

and that they satisfy a three-term recurrence relation. In particular, the q_j can be expressed as

$$q_j = \pi_j(A)\tilde{g}/\|\tilde{g}\|, \qquad j = 0, 1, 2, \ldots\ , \tag{15}$$

where π_j is a polynomial of degree j. We refer to the q_j as Lanczos vectors and to the π_j as Lanczos polynomials. Since the Lanczos vectors satisfy a tree-term recurrence relation, so do the Lanczos polynomials; see, e.g., Golub and Van Loan [8] for details on the Lanczos process.

We seek to determine an approximation of x_μ of the form

$$x_{\mu,m} = \sum_{j=0}^{m-1} \gamma_{j,m} q_j, \qquad \gamma_{j,m} \in \mathbb{R}. \tag{16}$$

In view of (12), the problem of approximating x_μ by $x_{\mu,m}$ is equivalent to the approximation of ψ_μ by a linear combination of the Lanczos polynomials (15). We will use this equivalence to derive a numerical method for determining the coefficients $\gamma_{j,m}$.

Our numerical method is based on the fact that the Lanczos polynomials are orthogonal with respect to an inner product defined by a measure on the real axis. A discussion on Lanczos polynomials and Gauss quadrature rules can be found in [7]. We review relevant properties and assume for simplicity that the Lanczos process does not break down until n steps have been carried out. Then Lanczos decompositions of the form (13) exist for $1 \leq m < n$. Moreover, when $m = n$, the vector q'_m in (13) vanishes and we obtain

$$A = Q_n T_n Q_n^*. \tag{17}$$

Substituting (17) into (12) gives

$$x_\mu = \psi_\mu(Q_n T_n Q_n^*)\tilde{g} = \|\tilde{g}\| Q_n \psi_\mu(T_n) e_1 = \sum_{j=0}^{n-1} \gamma_j q_j,$$

where

$$\gamma_j := \|\tilde{g}\| e_{j+1}^* \psi_\mu(T_n) e_1, \qquad 0 \le j < n. \tag{18}$$

Introduce the inner product

$$< f_1, f_2 >:= \frac{1}{\|\tilde{g}\|^2} (f_1(A)\tilde{g})^* (f_2(A)\tilde{g}) \tag{19}$$

for functions f_1 and f_2, such that the matrices

$$f_j(A) := U_n \mathrm{diag}[f_j(\lambda_1), f_j(\lambda_2), \ldots, f_j(\lambda_n)] U_n^*, \qquad j = 1, 2, \tag{20}$$

are well defined, where U_n and the λ_k are determined by (7). It follows from their definition (15) that the Lanczos polynomials are orthonormal,

$$< \pi_j, \pi_k >= \frac{1}{\|\tilde{g}\|^2} (\pi_j(A)\tilde{g})^* (\pi_k(A)\tilde{g}) = q_j^* q_k = \begin{cases} 1, & j = k, \\ 0, & j \ne k. \end{cases} \tag{21}$$

Consider the spectral decomposition

$$T_n = W_n \Lambda_n W_n^*, \qquad W_n^* W_n = I_n, \tag{22}$$

where the diagonal matrix Λ_n is the same as in (7). Analogously to (20), we define

$$f_j(T_n) := W_n \mathrm{diag}[f_j(\lambda_1), f_j(\lambda_2), \ldots, f_j(\lambda_n)] W_n^*, \qquad j = 1, 2, \tag{23}$$

and it follows from (17) that

$$f_j(A) = Q_n f_j(T_n) Q_n^*, \qquad j = 1, 2. \tag{24}$$

Substituting (24) and (23) into (19) yields

$$\begin{aligned} < f_1, f_2 > &= e_1^* f_1(T_n) f_2(T_n) e_1 \\ &= e_1^* W_n \mathrm{diag}[f_1(\lambda_1) f_2(\lambda_1), f_1(\lambda_2) f_2(\lambda_2), \ldots, f_1(\lambda_n) f_2(\lambda_n)] W_n^* e_1 \\ &= \sum_{j=1}^{n} f_1(\lambda_j) f_2(\lambda_j) \omega_j^2, \qquad \omega_j := e_1^* W_n e_j. \end{aligned} \tag{25}$$

Following Golub and Meurant [7], we write the sum (25) as a Stieltjes integral. For this purpose, define the nonnegative measure

$$d\omega(t) := \sum_{j=1}^{n} \delta(t - \lambda_j) \omega_j^2, \tag{26}$$

where δ denotes the Dirac δ-function. Then

$$< f_1, f_2 >= \sum_{j=1}^{n} f_1(\lambda_j) f_2(\lambda_j) \omega_j^2 = \int_{-\infty}^{\infty} f_1(t) f_2(t) d\omega(t). \tag{27}$$

We are now in a position to express the coefficients (18) in terms of Stieltjes integrals. It follows from (15) and (17) that

$$e_{j+1}^* \psi_\mu(T_n) e_1 = q_j^* \psi_\mu(A) q_0 = \frac{1}{\|\tilde{g}\|^2} (\pi_j(A)\tilde{g})^* (\psi_\mu(A)\tilde{g}) = < \pi_j, \psi_\mu > .$$

Substituting this expression into (18), and using the Stieltjes integral representation (27) for the inner product, yields

$$\gamma_j = \|\tilde{g}\| < \pi_j, \psi_\mu > = \|\tilde{g}\| \int_{-\infty}^{\infty} \pi_j(t)\psi_\mu(t) d\omega(t). \tag{28}$$

The evaluation of the coefficients γ_j by (18) or (28) requires that the matrix T_n or its eigenvalues and the first components of normalized eigenvectors be available. The computation of these quantities requires that n steps of the Lanczos process be carried out. However, this is not feasible when n is large. We therefore describe how approximations $\gamma_{j,m}$ of the coefficients γ_j for $0 \leq j < m$ can be computed when only $m < n$ steps of the Lanczos process have been carried out.

Introduce the spectral decomposition of the matrix T_m defined by (13),

$$T_m = W_m \Lambda_m W_m^*, \quad W_m^* W_m = I_m, \quad \Lambda_m = \mathrm{diag}[\lambda_{1,m}, \lambda_{2,m}, \ldots, \lambda_{m,m}], \tag{29}$$

and let

$$\omega_{j,m} := e_1^* W_m e_j, \qquad \breve{\omega}_{j,m} := e_m^* W_m e_j, \qquad 1 \leq j \leq m. \tag{30}$$

Analogously to (8), we introduce the index sets

$$\mathcal{J}_0(T_m) := \{j : \lambda_{j,m} = 0\}, \qquad \mathcal{J}_1(T_m) := \{j : \lambda_{j,m} \neq 0\}. \tag{31}$$

It is well known that the m-point Gauss quadrature rule associated with the measure (26) is given by

$$\mathcal{G}_m f := \sum_{j=1}^{m} f(\lambda_{j,m}) \omega_{j,m}^2; \tag{32}$$

see, e.g., [7]. We determine approximations $\gamma_{j,m}$ of the coefficients γ_j by replacing the Stieltjes integral in the right-hand side of (28) by the Gauss rule (32), i.e.,

$$\gamma_{j,m} := \|\tilde{g}\| \mathcal{G}_m(\pi_j \psi_\mu), \qquad 0 \leq j < m. \tag{33}$$

These coefficients and the Lanczos vectors $\{q_j\}_{j=0}^{m-1}$ define the approximation (16) of x_μ.

Analogously to the representation (18) of γ_j, we have

$$\gamma_{j,m} = \|\tilde{g}\| e_{j+1}^* \psi_\mu(T_m) e_1, \qquad 0 \leq j < m, \tag{34}$$

and substituting these expressions into (16) yields the representation

$$x_{\mu,m} = \|\tilde{g}\| Q_m \psi_\mu(T_m) e_1. \tag{35}$$

We remark that when increasing the number of steps m, the quality of the approximant $x_{\mu,m}$ of x_μ increases both because the size of the Krylov subspace in which

$x_{\mu,m}$ lives increases with m, and because the accuracy of the Gauss quadrature rules (33) increases with m for each fixed j. Bounds for $\|x_{\mu,m} - x_\mu\|$ can be derived as follows. Express the function $\psi_\mu(t)$ in $[a, b]$ as a series of Chebyshev polynomials of the first kind for this interval. Bounds for the oefficients in this expansion can be derived by techniques discussed in [5]. Since $\psi_\mu(t)$ is analytic in the finite complex plane, the terms in the series converge to zero faster than geometrically. Druskin and Knizhnerman [6] show how the bounds for these terms can be used to bound the error $\|x_{\mu,m} - x_\mu\|$. This approach shows that the error decreases faster than geometrically as m increases.

3. A modified iterative method. The representation (9) shows that x_μ is orthogonal to the null space of A. We describe a modification of the method of Section 2 with the property that the computed approximate solutions of (4), denoted by $\hat{x}_{\mu,m}$, also are orthogonal to the null space of A. Since the matrix A is symmetric, its null space and range are orthogonal. We therefore require the approximate solutions $\hat{x}_{\mu,m}$ to be in the range of A.

Let $\mathcal{R}(A)$ denote the range of A and define

$$\hat{g} := A\tilde{g}. \tag{36}$$

Apply m steps of the Lanczos process to the matrix A with initial vector $\hat{g}$. Assuming that the Lanczos process does not break down, we obtain, analogously to (13), the decomposition

$$A\hat{Q}_m = \hat{Q}_m\hat{T}_m + \hat{q}'_m e_m^*, \tag{37}$$

where the matrix $\hat{Q}_m = [\hat{q}_0, \hat{q}_1, \ldots, \hat{q}_{m-1}] \in \mathbb{R}^{n\times m}$ satisfies $\hat{Q}_m^*\hat{Q}_m = I_m$ and $\hat{Q}_m e_1 = \hat{g}/\|\hat{g}\|$, the matrix $\hat{T}_m \in \mathbb{R}^{m\times m}$ is symmetric and tridiagonal with nonvanishing subdiagonal elements, and the vector $\hat{q}'_m \in \mathbb{R}^n$ is orthogonal to the columns of $\hat{Q}_m$. It follows from (37) and (36) that the columns $\hat{q}_j$ of the matrix $\hat{Q}_m$ span the Krylov subspace $\mathcal{K}_m(A, A\tilde{g})$, which is in $\mathcal{R}(A)$.

We determine an approximation of x_μ of the form

$$\hat{x}_{\mu,m} = \sum_{j=0}^{m-1} \hat{\gamma}_{j,m}\hat{q}_j, \qquad \hat{\gamma}_{j,m} \in \mathbb{R}, \tag{38}$$

where we note that $\hat{x}_{\mu,m} \in \mathcal{R}(A)$ for any choice of coefficients $\hat{\gamma}_{j,m}$.

Introduce the function

$$\hat{\psi}_\mu(t) := \begin{cases} t^{-2}(1 - \exp(-\mu t^2)), & t \neq 0, \\ 0, & t = 0. \end{cases}$$

This function is discontinuous at $t = 0$ when $\mu \neq 0$. The solution (6) of the least-squares problem (4) can be expressed as

$$x_\mu = \hat{\psi}_\mu(A)\hat{g},$$

where we define $\hat{\psi}_\mu(A) := U_n \mathrm{diag}[\hat{\psi}_\mu(\lambda_1), \hat{\psi}_\mu(\lambda_2), \ldots, \hat{\psi}_\mu(\lambda_n)]U_n^*$.

Analogously to the representation (34) of the coefficients $\gamma_{j,m}$, we let

$$\hat{\gamma}_{j,m} := \|\hat{g}\| e_{j+1}^* \hat{\psi}_\mu(\hat{T}_m)e_1, \qquad 0 \leq j < m, \tag{39}$$

where $\hat{\psi}_\mu(\hat{T}_m)$ is defined similarly as $\hat{\psi}_\mu(A)$. Substituting (39) into (38) yields

$$\hat{x}_{\mu,m} = \|\hat{g}\|\hat{Q}_m\hat{\psi}_\mu(\hat{T}_m)e_1, \tag{40}$$

analogously to (35).

4. Determination of the regularization parameter. In many discrete ill-posed problems that arise in applications a suitable value of the regularization parameter μ is not known a priori. A method for determining such a value based on the discrepancy principle is described in [4]. This method requires that the norm of the noise e be known. The L-curve criterion for determining a suitable value of the regularization parameter, proposed by Hansen [12], does not require knowledge of $\|e\|$. This method is based on comparing the norm of the computed approximate solution with the norm of the associated residual vector. We focus primarily on the method of Section 2, which determines approximate solutions $x_{\mu,m}$ given by (35). The associated residual vector is defined by

$$r_{\mu,m} := \tilde{g} - Ax_{\mu,m}. \tag{41}$$

Before studying the behavior of $\|x_{\mu,m}\|$ and $\|r_{\mu,m}\|$ as a function of μ, we investigate how the norm of the solution x_μ of (4) and of the associated residual vector

$$r_\mu = \tilde{g} - Ax_\mu \tag{42}$$

changes with μ. Throughout this section $\mathcal{N}(A)$ denotes the null space of A.

THEOREM 4.1. *Let x_μ be defined by (6), let $\tilde{g}_{\mathcal{N}(A)}$ denote the orthogonal projection of $\tilde{g}$ onto $\mathcal{N}(A)$, and assume that $\tilde{g} \neq \tilde{g}_{\mathcal{N}}(A)$. Then the residual vector (42) associated with x_μ satisfies*

$$\|r_0\| = \|\tilde{g}\|, \tag{43}$$

$$\lim_{\mu\to\infty} \|r_\mu\| = \|\tilde{g}_{\mathcal{N}(A)}\|. \tag{44}$$

Moreover, $\|r_\mu\|$ is a strictly decreasing function of μ for $\mu \geq 0$.

Proof. Substituting the representation (9) into (42) yields

$$\begin{aligned} \|r_\mu\|^2 &= \sum_{j\in\mathcal{J}_0(A)} \delta_j^2 + \sum_{j\in\mathcal{J}_1(A)} (\delta_j - \phi_\mu(\lambda_j)\delta_j)^2 \\ &= \sum_{j\in\mathcal{J}_0(A)} \delta_j^2 + \sum_{j\in\mathcal{J}_1(A)} \exp(-2\mu\lambda_j^2)\delta_j^2, \end{aligned} \tag{45}$$

where the index sets $\mathcal{J}_0(A)$ and $\mathcal{J}_1(A)$ are defined by (8). Equations (43) and (44) follow from (45) and the observation that

$$\sum_{j\in\mathcal{J}_0(A)} \delta_j^2 = \|\tilde{g}_{\mathcal{N}(A)}\|^2.$$

Differentiating (45) with respect to μ yields

$$\|r_\mu\| \frac{d}{d\mu}\|r_\mu\| = -\sum_{j\in\mathcal{J}_1(A)} \lambda_j^2 \exp(-2\mu\lambda_j^2)\delta_j^2. \tag{46}$$

It follows from $\tilde{g} \neq \tilde{g}_{\mathcal{N}}(A)$ that the right-hand side of (46) is negative for $\mu \geq 0$, and therefore $\frac{d}{d\mu}\|r_\mu\| < 0$ for $\mu \geq 0$. Hence, $\|r_\mu\|$ is a strictly decreasing function of μ. ∎

THEOREM 4.2. *Let x_μ be defined by (6) for $\mu \geq 0$, and assume that $\tilde{g} \neq \tilde{g}_{\mathcal{N}(A)}$. Then*

$$\|x_0\| = 0, \tag{47}$$

$$\lim_{\mu\to\infty} \|x_\mu\| = \|A^\dagger \tilde{g}\|. \tag{48}$$

Moreover, $\|x_\mu\|$ is a strictly increasing function of μ for $\mu > 0$.

Proof. The representation (9) yields

$$\|x_\mu\|^2 = \sum_{j \in \mathcal{J}_1(A)} (1 - \exp(-\mu\lambda_j^2))^2 \left(\frac{\delta_j}{\lambda_j}\right)^2, \tag{49}$$

from which equations (47) and (48) follow. The condition $\tilde{g} \neq \tilde{g}_{\mathcal{N}}(A)$ secures that at least one term in the sum (49) is positive for $\mu > 0$. Differentiation of equation (49) with respect to μ shows that $\frac{d}{d\mu}\|x_\mu\| > 0$ for $\mu > 0$. □

We now show results analogous to Theorems 4.1 and 4.2 for the approximate solution (35) and the associated residual vector (41).

THEOREM 4.3. *The norm of the residual vector (41) can be expressed as*

$$\|r_{\mu,m}\| = (\|\exp(-\mu T_m^2)e_1\|^2 + |e_m^* \psi_\mu(T_m)e_1|^2 \|q'_m\|^2)^{1/2} \|\tilde{g}\|, \tag{50}$$

where the matrix T_m and vector q'_m are defined by the Lanczos decomposition (13). In particular,

$$\|r_{0,m}\| = \|\tilde{g}\|. \tag{51}$$

If the vector q'_m in the Lanczos decomposition (13) vanishes, then $\|r_{\mu,m}\|$ is a decreasing function of μ for $\mu \geq 0$, and

$$\lim_{\mu \to \infty} \|r_{\mu,m}\| = (\sum_{j \in \mathcal{J}_0(T_m)} \omega_{j,m}^2)^{1/2} \|\tilde{g}\|, \tag{52}$$

where the index set $\mathcal{J}_0(T_m)$ is defined by (31) and the Gaussian weights $\omega_{j,m}^2$ are determined by (30). In particular, when T_m is nonsingular, $\mathcal{J}_0(T_m) = \emptyset$ and $\lim_{\mu \to \infty} \|r_{\mu,m}\| = 0$.

Conversely, if $q'_m \neq 0$, then

$$\lim_{\mu \to \infty} \|r_{\mu,m}\| = (\sum_{j \in \mathcal{J}_0(T_m)} \omega_{j,m}^2 + |e_m^* T_m^\dagger e_1|^2 \|q'_m\|^2)^{1/2} \|\tilde{g}\|. \tag{53}$$

Since $e_m^* T_m^\dagger e_1 \neq 0$, the norm of $r_{\mu,m}$ might not be a decreasing function of μ.

Proof. Substituting (35) and (13) into (41) yields

$$r_{\mu,m} = \tilde{g} - AQ_m \psi_\mu(T_m)e_1 \|\tilde{g}\| = (Q_m(I_m - T_m\psi_\mu(T_m))e_1 - q'_m e_m^* \psi_\mu(T_m)e_1)\|\tilde{g}\|.$$

The orthogonality of the vector q'_m to the columns of Q_m yields (50). Substituting the spectral decomposition (29) of T_m into (50) gives

$$\begin{aligned} \|r_{\mu,m}\|^2 = (&\sum_{j \in \mathcal{J}_1(T_m)} \exp(-2\mu\lambda_{j,m}^2)\omega_{j,m}^2 + \sum_{j \in \mathcal{J}_0(T_m)} \omega_{j,m}^2)\|\tilde{g}\|^2 \\ &+ (\sum_{j \in \mathcal{J}_1(T_m)} \breve{\omega}_{j,m}\omega_{j,m}\psi_\mu(\lambda_{j,m}))^2 \|q'_m\|^2 \|\tilde{g}\|^2, \end{aligned} \tag{54}$$

where the $\omega_{j,m}$ and $\breve{\omega}_{j,m}$ are given by (30). Setting $q'_m = 0$ in this expression shows (51) and (52). Moreover, it follows from (54) that $\|r_{\mu,m}\|$ is a decreasing function of μ when $q'_m = 0$.

Since the sub- and super-diagonal entries of T_m are nonvanishing, it is easy to see that the first and last eigenvector components $\omega_{j,m}$ and $\breve{\omega}_{j,m}$, given by (30), are

nonvanishing for all j. Therefore, the last term in (54) does not vanish when $q'_m \neq 0$. The observation that

$$\lim_{\mu\to\infty} \sum_{j\in\mathcal{J}_1(T_m)} \breve{\omega}_{j,m}\omega_{j,m}\psi_\mu(\lambda_{j,m}) = \lim_{\mu\to\infty} \sum_{j\in\mathcal{J}_1(T_m)} \breve{\omega}_{j,m}\omega_{j,m}\lambda_{j,m}^{-1} = e_m^* T_m^\dagger e_1$$

completes the proof. □

We have observed in computations that typically $\|r_{\mu,m}\|$ decreases monotonically for $0 \leq \mu \leq \mu_*$ for some $\mu_* > 0$. For large values of μ, the norm of $r_{\mu,m}$ may increase with μ. This is illustrated by computed examples in Section 5.

THEOREM 4.4. *Let $x_{\mu,m}$ be given by (35) for $\mu \geq 0$. Then*

$$\|x_{0,m}\| = 0, \tag{55}$$

$$\lim_{\mu\to\infty} \|x_{\mu,m}\| = \|\tilde{g}\|(e_1^*(T_m^\dagger)^2 e_1)^{1/2}. \tag{56}$$

Moreover, $\|x_{\mu,m}\|$ is a strictly increasing function of μ for $\mu > 0$.

Proof. The representation (35) of $x_{\mu,m}$ yields

$$\|x_{\mu,m}\|^2 = \|\psi_\mu(T_m)e_1\|^2\|\tilde{g}\|^2 = \sum_{j\in\mathcal{J}_1(T_m)} \lambda_{j,m}^{-2}(1-\exp(-\mu\lambda_{j,m}^2))^2\omega_{j,m}^2\|\tilde{g}\|^2. \tag{57}$$

Equation (55) follows by setting $\mu = 0$ in (57). Letting $\mu \to \infty$ in (57) yields

$$\lim_{\mu\to\infty} \|x_{\mu,m}\|^2 = \sum_{j\in\mathcal{J}_1(T_m)} \lambda_{j,m}^{-2}\omega_{j,m}^2\|\tilde{g}\|^2,$$

which shows (56). Differentiation of (57) with respect to μ shows that $\frac{d}{d\mu}\|x_{\mu,m}\| > 0$ for $\mu > 0$. □

Results analogous to those of Theorems 4.3 and 4.4 can be established for the approximate solution $\hat{x}_{\mu,m}$ defined by (40) and the associated residual vector $\hat{r}_{\mu,m} := \tilde{g} - A\hat{x}_{\mu,m}$. For instance, the following properties of $\hat{x}_{\mu,m}$ can be shown similarly as Theorem 4.4.

THEOREM 4.5. *Let $\hat{x}_{\mu,m}$ be defined by (40) for $\mu \geq 0$. Then*

$$\|\hat{x}_{0,m}\| = 0,$$

$$\lim_{\mu\to\infty} \|\hat{x}_{\mu,m}\| = \|\hat{g}\|(e_1^*(T_m^\dagger)^4 e_1)^{1/2}.$$

Moreover, $\|\hat{x}_{\mu,m}\|$ is a strictly increasing function of μ for $\mu > 0$.

We turn to the determination of a suitable value of the regularization parameter. Hansen [12] proposed a simple approach known as the L-curve criterion. We describe how this criterion conveniently can be applied to determine a suitable value of the regularization parameter for the iterative method of Section 2. The L-curve criterion can be applied to the method of Section 3 in a similar fashion.

Let $x_{\mu,m}$ and $r_{\mu,m}$ be given by (35) and (41), respectively, and consider the point set

$$\mathcal{L} := \{(\|x_{\mu,m}\|, \|r_{\mu,m}\|) : \mu > 0\}. \tag{58}$$

In the numerical experiments of Section 5, we plot this set in a log-log scale. The graph so obtained is convex for many linear discrete ill-posed problems (1), in agreement

with Theorems 4.3 and 4.4. For small values of μ the slope of the graph is negative and of large magnitude. This indicates that an increase of μ gives a significant reduction in the norm $\|r_{\mu,m}\|$, but $\|x_{\mu,m}\|$ only increases slightly. For larger values of μ, the graph typically has a negative slope of small magnitude. This indicates that an increase of μ only gives a slight decrease of $\|r_{\mu,m}\|$, but $\|x_{\mu,m}\|$ may grow considerably. For even larger values of μ both $\|r_{\mu,m}\|$ and $\|x_{\mu,m}\|$ might increase with μ.

When the vector $q'_m = 0$, $\|r_{\mu,m}\|$ is a decreasing function of μ, cf. Theorem 4.3, and the graph of the set $\mathcal{L}$ often looks like the letter "L". Theorem 4.3 indicates that when $q'_m \neq 0$, the graph may be shaped like the letter "U". We refer to the graph of the set $\mathcal{L}$ as the L-curve, whether q'_m vanishes or not. Following the approach by Hansen [12], we choose a value of the regularization parameter in the vicinity of the point of largest curvature of the graph. The value of μ so determined seeks to achieve a small norm of the residual vector $r_{\mu,m}$ and a fairly small norm of the computed approximate solution $x_{\mu,m}$. If the graph is "U-shaped" in the vicinity of the point of largest curvature, then it may be possible to reduce the error $x_{\mu.m} - x'$ by increasing the value of m.

We remark that the L-curve criterion may fail to determine a suitable value of the regularization parameter for certain problems. However, its simplicity and the fact that it for many problems gives a fairly good value of the the regularization parameter contribute to its popularity. For insightful discussions on the advantages and limitations of the L-curve criterion, we refer to [14, 15].

5. Computed examples. This section describes numerical examples that illustrate the performance of the exponential filtering method of Section 2. The method of Section 3 performed in a similar manner. We therefore do not report experiments with the latter method. The only advantage of the method of Section 3 is that the approximate solutions determined are guaranteed to be orthogonal to the null space of A.

Our implementation of the exponential filtering method of Section 2 stores the matrix Q_m and vector q'_m in the Lanczos decomposition (13), and reorthogonalizes the columns of Q_m and q'_m to secure numerical orthogonality. We compare this implementation with the MR-II method proposed by Hanke and use the implementation described in [9]. The MR-II method is a minimal residual method that determines a sequence of approximate solutions $\breve{x}_m \in \mathcal{K}_m(A, A\tilde{g})$ of (1) that satisfy

$$\|A\breve{x}_m - \tilde{g}\| = \min_{x \in \mathcal{K}_m(A,A\tilde{g})} \|Ax - \tilde{g}\|, \qquad m = 1, 2, \ldots \ .$$

The iteration number m can be thought of as the regularization parameter. It is important to determine when to terminate the iterations with the MR-II method. Too few iterations gives a residual vector $\breve{r}_m := \tilde{g} - A\breve{x}_m$ of unnecessarily large norm, and too many iterations yields an approximate solution $\breve{x}_m$ that is severely contaminated by propagated errors due to the error e in the right-hand side $\tilde{g}$. An analysis of the performance of the MR-II method is provided by Hanke [9]. The MR-II method only requires storage of a few n-vectors at a time.

The point set

$$\mathcal{L}_d := \{(\|\breve{x}_m\|, \|\breve{r}_m\|) : m = 1, 2, \ldots \ \} \tag{59}$$

determined by the iterates $\breve{x}_m$ and associated residual vectors $\breve{r}_m$ generated by the MR-II method is analogous to the set (58) for the exponential filtering method of Section 2. Below we show log-log plots of the curves obtained by linear interpolation

between successive points in the set (59) and refer to these graphs as L-curves for the MR-II method. For many linear discrete ill-posed problems (1) these graphs are shaped like the letter "L". Iterates $\breve{x}_m$ associated with points close to the "vertex" of the graph are often suitable choices of approximate solutions of (1). This approach of choosing the regularization parameter for iterative methods is discussed in [10, 11, 14].

We found that for many linear discrete ill-posed problems (1) the best possible approximations of the minimal-norm least-squares solution of the associated noise-free linear system of equations (3), denoted by x', determined by the method of Section 2 and by the MR-II method are of roughly the same quality. Moreover, the value of the regularization parameter μ determined by the L-curve (58) and the number of iterations m determined by the L-curve for the MR-II method (59) often are adequate. Example 5.1 below provides an illustration. However, for some linear discrete ill-posed problems, the exponential filtering method of Section 2 implemented as described in the present section gives considerably better approximations of x' than the MR-II method. This is illustrated by Example 5.2.

All computed examples of this section are implemented in Matlab on a PC with a Pentium III processor. The unit roundoff is $\epsilon \approx 2 \cdot 10^{-16}$.

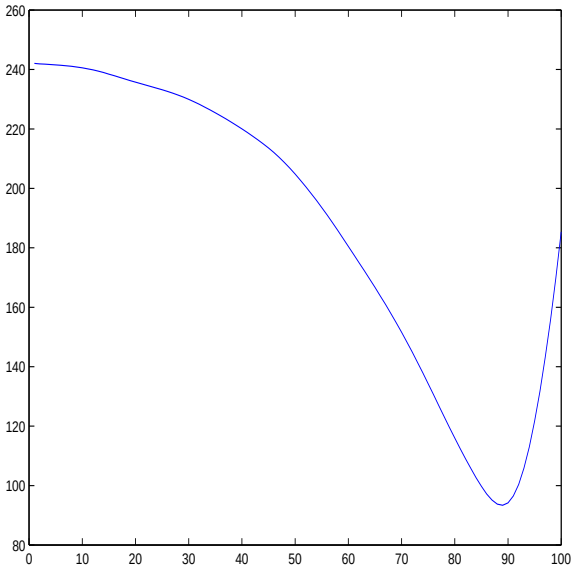

FIG. 1. *Example 5.1: Error $\|x_{\mu_j,60} - x'\|$ as a function of j for approximate solutions $x_{\mu_j,60}$ determined by the exponential filtering method, where $\mu_j := 100 \cdot (1.25)^{j-1}$, $1 \leq j \leq 100$.*

Example 5.1. We are concerned with the solution of a linear system of equations of the form (1) with the matrix defined by

$$A := U_{300}\Lambda_{300}U_{300}^* \in \mathbb{R}^{300\times 300},$$

where

$$\Lambda_{300} := \mathrm{diag}[1, 2^{-3}, 3^{-3}, \ldots, 300^{-3}], \tag{60}$$

and U_{300} is the orthogonal eigenvector matrix of a symmetric 300×300 matrix determined by discretizing a Fredholm integral equation of the first kind discussed by

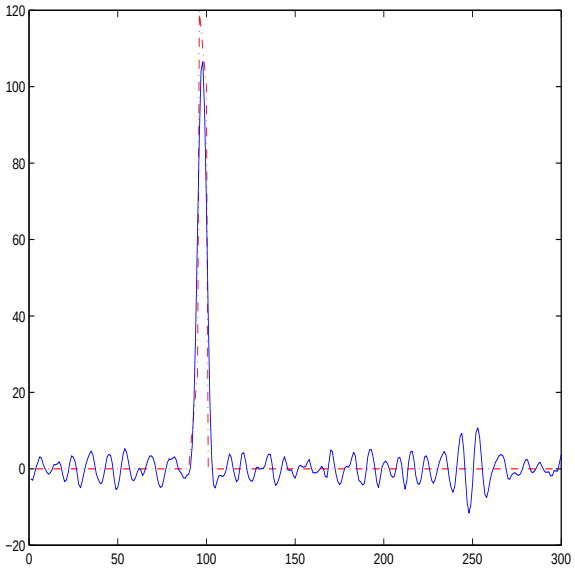

FIG. 2. *Example 5.1: Computed approximate solution $x_{\mu_{89},60}$ by the exponential filtering method (continuous curve) and exact solution x' of the noise-free linear system (3) (dash-dotted curve).*

Phillips [17]. The discretization was carried out using Matlab code provided by Hansen [13]. The eigenvectors u_j have the property that the number of sign changes in the sequence $\{e_j^* u_k\}_{j=1}^{300}$ increases with the index k. This property is typical of matrices obtained by discretizing Fredholm integral equations of the first kind.

Let $x' \in \mathbb{R}^{300}$ represent the spike shown by the dash-dotted graph in Figure 2; only 10 of the entries of the vector are nonvanishing. Define the noise-free right-hand side $g' := Ax'$. Then $\|x'\| = 2.5 \cdot 10^2$ and $\|g'\| = 4.3 \cdot 10^1$. Let the entries of the noise-vector e be normally distributed with zero mean and variance chosen so that $\|e\| = 1 \cdot 10^{-3}$ and define the contaminated right-hand side by $\tilde{g} := g' + e$, cf. (2).

First consider the exponential filtering method of Section 2. We carry out 60 steps of the Lanczos process and evaluate the norms of the approximate solutions $x_{\mu_j,60}$ and of the associated residual vectors $r_{\mu_j,60}$ for $\mu_j := 100 \cdot 1.25^{j-1}$, $1 \leq j \leq 100$. After the Lanczos decomposition (13) with $m = 60$ has been computed, we determine the spectral decomposition (29) of the symmetric tridiagonal matrix T_{60} generated by the Lanczos process. The norms $\|r_{\mu_j,60}\|$ and $\|x_{\mu_j,60}\|$ can then be computed quite inexpensively for each value of μ_j by using the formulas (54) and (57).

Figure 1 displays the error $\|x_{\mu_j,60} - x'\|$ for $\mu_j := 100 \cdot 1.25^{j-1}$ and $1 \leq j \leq 100$. The smallest error is achieved for $j = 89$; we have $\mu_{89} = 3.4 \cdot 10^{10}$. The continuous graph of Figure 2 displays $x_{\mu_{89},60}$, the dash-dotted curve shows x'. The latter figure shows $x_{\mu_{89},60}$ to be a fairly good approximation of x'. We have $\|x_{\mu_{89},60} - x'\| = 9.3 \cdot 10^1$.

Figure 3 shows the L-curve (58) for $m = 60$ and $\mu_j := 100 \cdot 1.25^{j-1}$, $1 \leq j \leq 100$. We have marked the point $(\|x_{\mu_{89},60}\|, \|r_{\mu_{89},60}\|)$ on the L-curve by "$*$". This point is located near the point of largest curvature of the L-curve. Thus, the value of the regularization parameter μ associated with the point of largest curvature on the L-curve is appropriate for linear system of equations of the present example.

We turn to the MR-II method and compute approximate solutions $\breve{x}_m$ for $1 \leq$

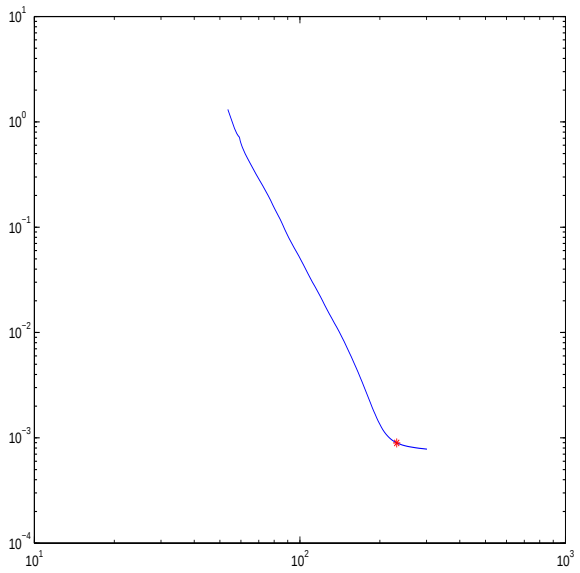

FIG. 3. *Example 5.1: L-curve (58) for the exponential filtering method for* $m = 60$ *and* $\mu = \mu_j = 10 \cdot 1.25^{j-1}$, $1 \leq j \leq 100$. *The point* $(\|x_{\mu_{89},60}\|, \|r_{\mu_{89},60}\|)$ *on the curve is marked by "*".*

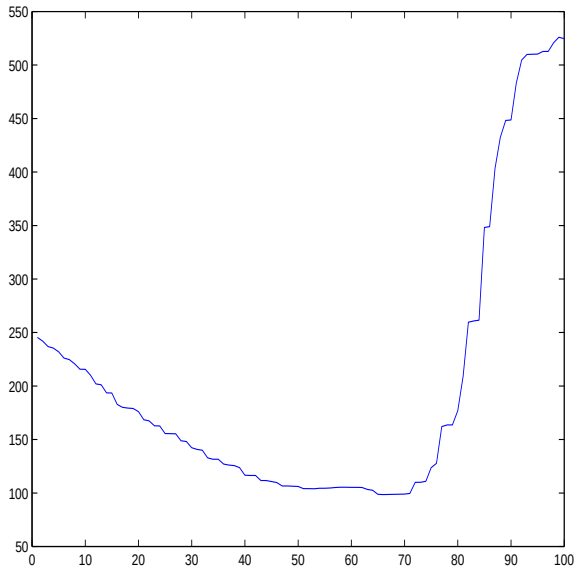

FIG. 4. *Example 5.1: Error* $\|\breve{x}_m - x'\|$ *as a function of* m, $1 \leq m \leq 100$, *for solutions* $\breve{x}_m$ *determined by the MR-II method.*

$m \leq 100$. Figure 4 shows the error $\|\breve{x}_m - x'\|$ for $1 \leq m \leq 100$. The smallest error is achieved for $m = 66$. Figure 5 shows the computed solution $\breve{x}_{66}$ (continuous curve) and the exact solution x' of the noise-free linear system of equations (3) (dash-dotted curve). The figure shows $\breve{x}_{66}$ to be a fairly good approximation of x'; we have $\|\breve{x}_{66} - x'\| = 9.9 \cdot 10^1$. This error is slightly larger than the error for the approximate

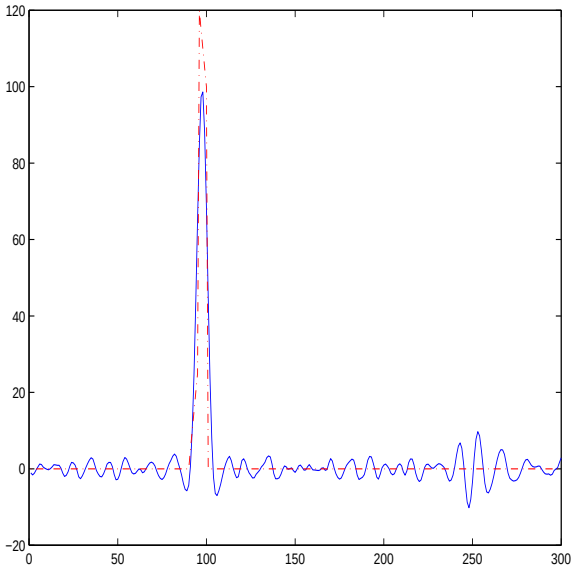

FIG. 5. *Example 5.1: Computed approximate solution $\breve{x}_{66}$ by the MR-II method (continuous curve) and exact solution x' of the noise-free linear system (3) (dash-dotted curve).*

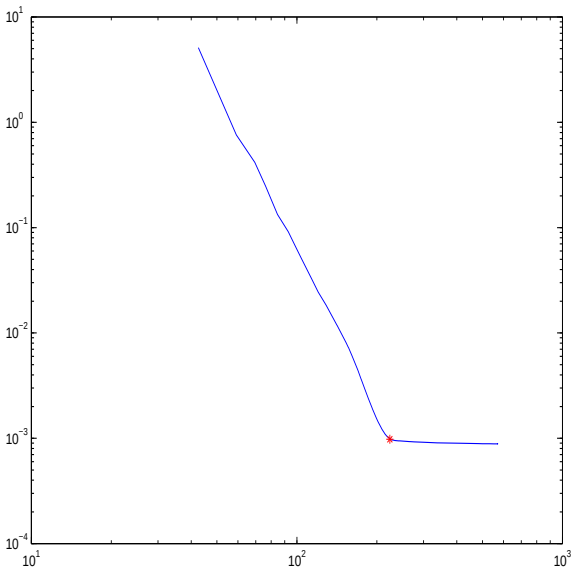

FIG. 6. *Example 5.1: L-curve for the MR-II method defined by the set (59) for $1 \leq m \leq 100$. Adjascent points are connected by straight lines. The point $(\|\breve{x}_{66}\|, \|\breve{r}_{66}\|)$ is marked by "$*$".*

solution $x_{\mu_{89},60}$ determined by the exponential filtering method.

Figure 6 displays the L-curve associated with the MR-II method. The point $(\|\breve{x}_{66}\|, \|\breve{r}_{66}\|)$ is marked by "$*$". It is located at a point where the slope of the L-curve for the MR-II method changes the most, i.e., at the "vertex" of the L-curve. □

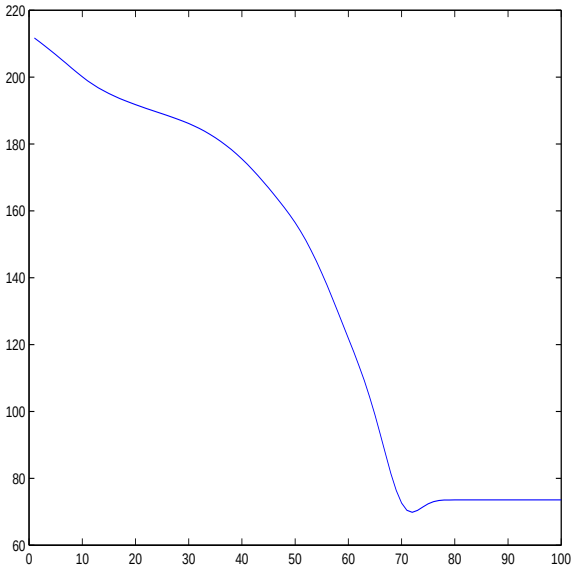

FIG. 7. *Example 5.2: Error* $\|x_{\mu_j,40} - x'\|$ *as a function of* j *for approximate solutions* $x_{\mu_j,40}$ *determined by the exponential filtering method, where* $\mu_j := 10^7 \cdot (1.25)^{j-1}$, $1 \leq j \leq 100$.

Example 5.2. The matrix A in this example has the same eigenvalues as the matrix in Example 5.1, but has a different eigenvector matrix. Thus, let Λ_{300} be defined by (60) and let U_{300} be the orthogonal eigenvector matrix of a symmetric 300×300 matrix determined by discretizing a Fredholm integral equation of the first kind discussed by Shaw [18]. The discretization was carried out using Matlab code provided by Hansen [13]. The eigenvectors u_j have the property that the number of sign changes in the sequence $\{e_j^* u_k\}_{j=1}^{300}$ increases with the index k. We define $A := U_{300}\Lambda_{300}U_{300}^*$. Let the vector x' be the same as in Example 5.1 and introduce $g' := Ax'$. Thus, g' is the right-hand side and x' the solution of the noise-free linear system of equations (3). Divide the noise vector used in Example 5.1 by 100. This gives a noise vector e of norm $1 \cdot 10^{-5}$. Define the right-hand side of the linear system (1) by $\tilde{g} := g' + e$.

We first consider the exponential filtering method of Section 2. Carry out 40 steps of the Lanczos process and evaluate the norms of the approximate solutions $x_{\mu_j,40}$ and of the associated residual vectors $r_{\mu_j,40}$ for $\mu_j := 1 \cdot 10^7 \cdot 1.25^{j-1}$, $1 \leq j \leq 100$.

Figure 7 displays $\|x_{\mu_j,40} - x'\|$ for $1 \leq j \leq 100$ and shows that the smallest error is achieved for $j = 72$, which corresponds to the value $\mu_{72} = 7.6 \cdot 10^{13}$ of the regularization parameter. The continuous curve of Figure 8 displays $x_{\mu_{72},40}$ and the dash-dotted curve shows the exact solution of the noise-free system x'. The figure shows $x_{\mu_{72},40}$ to be a fairly good approximation of x'. We have $\|x_{\mu_{72},40} - x'\| = 7.0 \cdot 10^1$.

Figure 9 shows the L-curve (58) with $m = 40$. The point $(\|x_{\mu_{72},40}\|, \|r_{\mu_{72},40}\|)$ on the L-curve is marked by "$*$". The L-curve is seen to be "U-shaped" and the star "$*$" is located slightly to the right of the point of largest curvature on the L-curve. In fact, the point of largest curvature is roughly at $\mu = \mu_{70}$. Figure 7 indicates that $x_{\mu_{70},40}$ approximates x' almost as well as $x_{\mu_{72},40}$. Thus, in this example the point of largest curvature of the L-curve determines a suitable value of the regularization parameter.

The U-shape of the L-curve indicates that a better approximation of x' may

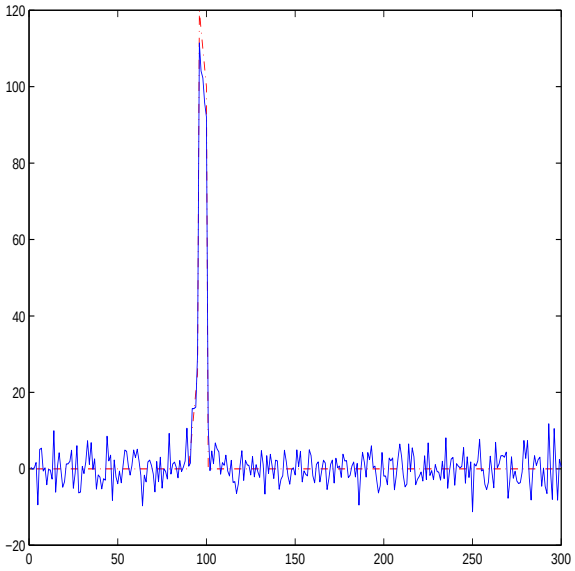

FIG. 8. *Example 5.2: Computed approximate solution $x_{\mu_{72},40}$ by the exponential filtering method (continuous curve) and exact solution x' of the noise-free linear system (3) (dash-dotted curve).*

be achievable by increasing the number of Lanczos steps. Thus, in an interactive computing environment, the L-curve (58) can be used both to determine a suitable value of the regularization parameter μ and an appropriate number of Lanczos steps m. We would like m to be large enough to make the L-curve L-shaped rather than U-shaped in a vicinity of the point of largest curvature. Nevertheless, in the present example $m = 40$ Lanczos steps suffices to determine an approximation of x' that is substantially better than the best approximation computed by the MR-II method. We computed the approximate solutions $\breve{x}_m$, $1 \leq m \leq 100$, by the latter method. The smallest error $\|\breve{x}_m - x'\|$ is achieved for $m = 50$; it is $\|\breve{x}_{50} - x'\| = 1.9 \cdot 10^2$. Figure 10 shows the computed solution $\breve{x}_{50}$ (continuous curve) and the exact solution of the noise-free system x' (dash-dotted curve).

Figure 11 displays the L-curve (59) associated with the MR-II method. The point $(\|\breve{x}_{50}\|, \|\breve{r}_{50}\|)$ is marked by "$*$". Note that $\|\breve{x}_m\|$ does not grow monotonically with m and therefore the L-curve is not L-shaped. The possibility of the L-curve for the MR-II method not being L-shaped has previously been pointed out in [2], and another L-curve was proposed there. However, since the MR-II method only achieves poor approximations of the vector x' in the present example we do not dwell on alternative L-curves in this paper.

In exact arithmetic, without round-off errors, the search directions generated by the MR-II method are A^2-conjugate. The reason for the poor performance of the MR-II method in this example is that this property is violated by the computed search directions due to propagated round-off errors. Other implementations of the MR-II method may perform better, however, the discussion of implementation issues of the MR-II method is outside the scope of the present paper. Here we only note that the exponential filtering method of Section 2 implemented as described in the beginning of this section may yield significantly better approximations of x' than the standard

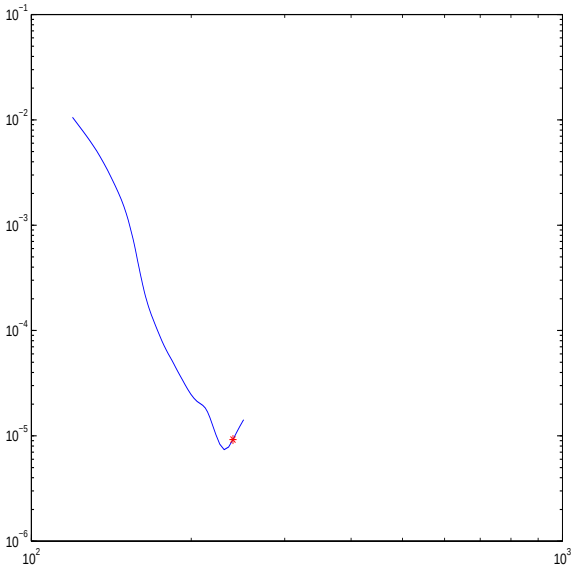

FIG. 9. *Example 5.2: L-curve (58) for the exponential filtering method for* $m = 40$ *and* $\mu_j = 1 \cdot 10^7 \cdot 1.25^{j-1}$, $1 \leq j \leq 100$. *The point* $(\|x_{\mu_{72},40}\|, \|r_{\mu_{72},40}\|)$ *on the L-curve is marked by "*$*$*".*

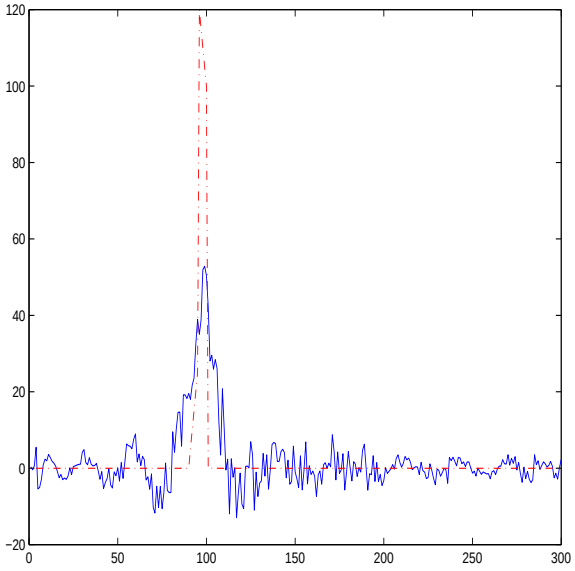

FIG. 10. *Example 5.2: Computed approximate solution* $\breve{x}_{50}$ *by MR-II method (continuous curve) and exact solution* x' *of the noise-free linear system (3) (dash-dotted curve).*

implementation of the MR-II method described in [9]. □

6. Conclusion. This paper describes an exponential filtering method based on the Lanczos process. Similarly as Tikhonov regularization, the method depends on a regularization parameter that can be varied continuously. Our numerical experience suggests that the L-curve (58) often is a useful aid for determining a suitable value

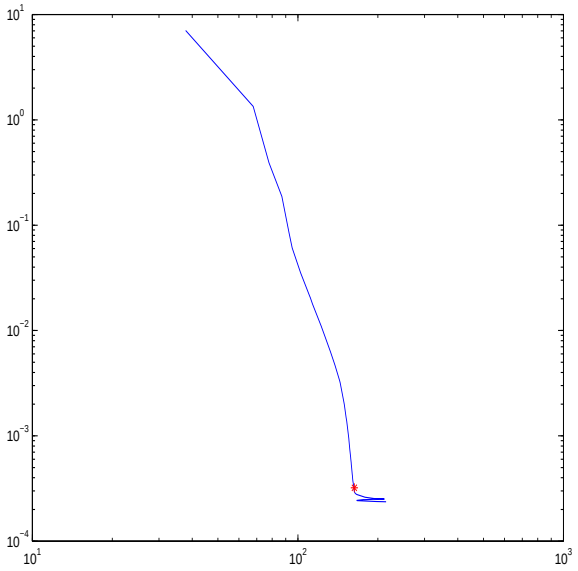

FIG. 11. *Example 5.2: L-curve for the MR-II method defined by the set (59) for* $1 \leq m \leq 100$. *Adjascent points are connected by straight lines. The point* $(\|\breve{x}_{50}\|, \|\breve{r}_{50}\|)$ *is marked by "*".*

of the regularization parameter and an appropriate number of Lanczos steps for the exponential filtering method.

REFERENCES

[1] D. Calvetti, B. Lewis and L. Reichel, Smooth or abrupt: a comparison of regularization methods, in Advanced Signal Processing Algorithms, Architectures and Implementations VIII, ed. F. T. Luk, Proceedings of the Society of Photo-Optical Instrumentation Engineers (SPIE), vol. 3461, The International Society for Optical Engineering, Bellingham, WA, 1998, pp. 286–295.

[2] D. Calvetti, B. Lewis and L. Reichel, An L-curve for the MINRES method, in Advanced Signal Processing Algorithms, Architectures, and Implementations X, ed. F. T. Luk, Proceedings of the Society of Photo-Optical Instrumentation Engineers (SPIE), vol. 4116, The International Society for Optical Engineering, Bellingham, WA, 2000, pp. 385–395.

[3] D. Calvetti, L. Reichel and Q. Zhang, Iterative solution methods for ill-posed problems, in Advanced Signal Processing Algorithms, ed. F. T. Luk, Proceedings of the Society of Photo-Optical Instrumentation Engineers (SPIE), vol. 2563, The International Society for Optical Engineering, Bellingham, WA, 1995, pp. 338–347.

[4] D. Calvetti, L. Reichel and Q. Zhang, Iterative exponential filtering for large discrete ill-posed problems, Numer. Math., 83 (1999), pp. 535–556.

[5] D. Calvetti, L. Reichel and Q. Zhang, Iterative solution methods for large linear discrete ill-posed problems, Applied and Computational Control, Signals and Circuits, 1 (1999), pp. 313–367.

[6] V. L. Druskin and L. Knizhnerman, Two polynomial methods of calculating functions of a symmetric matrix, U. S. S. R. Comput. Math. Math. Phys., 29 (6) (1989), pp. 112–121.

[7] G. H. Golub and G. Meurant, Matrices, moments and quadrature, in Numerical Analysis 1993, eds. D. F. Griffins and G. A. Watson, Longman, Essex, England, 1994, pp. 105–156.

[8] G. H. Golub and C. F. Van Loan, Matrix Computations, 3rd ed., Johns Hopkins University Press, Baltimore, 1996.

[9] M. Hanke, Conjugate Gradient Type Methods for Ill-Posed Problems, Longman, Harlow, 1995.

[10] M. Hanke and P. C. Hansen, Regularization methods for large-scale problems, Surv. Math. Ind., 3 (1993), pp. 253–315.

[11] M. Hanke and J. G. Nagy, Restoration of atmospherically blurred images by symmetric indefi-

nite conjugate gradient techniques, Inverse Problems, 12 (1996), pp. 157–173.
[12] P. C. Hansen, Analysis of discrete ill-posed problems by means of the L-curve, SIAM Review, 34 (1992), pp. 561–580.
[13] P. C. Hansen, Regularization tools: A Matlab package for analysis and solution of discrete ill-posed problems, Numer. Algorithms, 6 (1994), pp. 1–35.
[14] P. C. Hansen, Rank Deficient and Discrete Ill-Posed Problems, SIAM, Philadelphia, 1998.
[15] P. C. Hansen, The L-curve and its use in the numerical treatment of inverse problems, in Advances in Biomedicine, vol. 4, ed. P. Johnston, WIT Press, Southampton, England, 2000, pp. 119–142.
[16] A. K. Louis, A unified approach to regularization methods for linear ill-posed problems, Inverse Problems, 15 (1999), pp. 489–498.
[17] D. L. Phillips, A technique for the numerical solution of certain integral equations of the first kind, J. ACM, 9 (1962), pp. 84–97.
[18] C. B. Shaw, Jr., Improvements of the resolution of an instrument by numerical solution of an integral equation, J. Math. Anal. Appl., 37 (1972), pp. 83–112.